



## Continuously distributed magnetization profile for millimeter-scale elastomeric undulatory swimming

Eric Diller, Jiang Zhuang, Guo Zhan Lum, Matthew R. Edwards, and Metin Sitti

Citation: [Applied Physics Letters](#) **104**, 174101 (2014); doi: 10.1063/1.4874306

View online: <http://dx.doi.org/10.1063/1.4874306>

View Table of Contents: <http://scitation.aip.org/content/aip/journal/apl/104/17?ver=pdfcov>

Published by the [AIP Publishing](#)

---

### Articles you may be interested in

[Magnetic approaches to study collective three-dimensional cell mechanics in long-term cultures \(invited\)](#)

*J. Appl. Phys.* **115**, 172616 (2014); 10.1063/1.4870918

[Formation and magnetic manipulation of periodically aligned microchains in thin plastic membranes](#)

*J. Appl. Phys.* **112**, 083927 (2012); 10.1063/1.4759328

[The incorporation of the Cauchy stress matrix tensor in micromagnetic simulations](#)

*J. Appl. Phys.* **108**, 073903 (2010); 10.1063/1.3489969

[Magnetic micromachines prepared by ferrite plating technique](#)

*J. Appl. Phys.* **93**, 6712 (2003); 10.1063/1.1556928

[Rapid prototyping of active microfluidic components based on magnetically modified elastomeric materials](#)

*J. Vac. Sci. Technol. B* **19**, 596 (2001); 10.1116/1.1350840

---

**NEW! Asylum Research MFP-3D Infinity™ AFM**  
Unmatched Performance, Versatility and Support

**OXFORD INSTRUMENTS**  
*The Business of Science®*

Stunning high performance

Simpler than ever to GetStarted™

Comprehensive tools for nanomechanics

Widest range of accessories for materials science and bioscience

The advertisement features a dark blue background with white and orange text. It includes several images: a textured surface, a brownish material, a grid of small components, and the Asylum Research MFP-3D Infinity AFM instrument. The Oxford Instruments logo is in the top right corner.



## Continuously distributed magnetization profile for millimeter-scale elastomeric undulatory swimming

Eric Diller,<sup>1,2,a)</sup> Jiang Zhuang,<sup>1,a)</sup> Guo Zhan Lum,<sup>1,3</sup> Matthew R. Edwards,<sup>1</sup> and Metin Sitti<sup>1,b)</sup>

<sup>1</sup>Department of Mechanical Engineering, Carnegie Mellon University, Pittsburgh, Pennsylvania 15213, USA

<sup>2</sup>Department of Mechanical and Industrial Engineering, University of Toronto, Toronto M5S 3G8, Canada

<sup>3</sup>School of Mechanical and Aerospace Engineering, Nanyang Technological University, Singapore 639798

(Received 6 March 2014; accepted 21 April 2014; published online 29 April 2014)

We have developed a millimeter-scale magnetically driven swimming robot for untethered motion at mid to low Reynolds numbers. The robot is propelled by continuous undulatory deformation, which is enabled by the distributed magnetization profile of a flexible sheet. We demonstrate control of a prototype device and measure deformation and speed as a function of magnetic field strength and frequency. Experimental results are compared with simple magnetoelastic and fluid propulsion models. The presented mechanism provides an efficient remote actuation method at the millimeter scale that may be suitable for further scaling down in size for micro-robotics applications in biotechnology and healthcare. © 2014 AIP Publishing LLC.

[<http://dx.doi.org/10.1063/1.4874306>]

Untethered mobile micro-robots have the potential to contribute to radical advances in biomedical engineering and research due to their ability to operate effectively in small environments with limited accessibility.<sup>1,2</sup> Micron-scale actuation and control in liquid environments have been addressed by a number of different methods, including propulsion by swimming microorganisms and contractile cells;<sup>3–6</sup> steering via taxis behaviors of the microorganisms;<sup>3,7,8</sup> actuation by chemical reaction<sup>9</sup> and on-off control by pH;<sup>10</sup> and integrated actuation and control by remotely delivered magnetic fields.<sup>11–15</sup> Magnetic field propulsion is of particular importance because it can provide long-range direct control over both force and torque independently, allowing for a variety of propulsion techniques to be developed. It has been shown that the most efficient method to drive a magnetic device at size scales below 1 mm in a liquid medium is to employ a swimming gait based on magnetic torque actuation instead of using field gradients to directly pull the device.<sup>16</sup>

Micro-scale swimmers are subject to a different balance of fluid forces than their large-scale counterparts, which dictates the design and propulsion used. The Reynolds number ( $Re$ ) gives the ratio of inertial to viscous forces for a given flow condition and is crucial for determining fluid behavior at different size scales. Robots below the millimeter-scale in liquid environments are generally operating in the low- $Re$  regime with negligible inertial fluid effects, and thus are subject to restrictions on the kinds of motion that can generate net propulsive force. In order to move in low- $Re$ , or Stokes flow, the driving deformation of the device must not be time-symmetric.<sup>17</sup> We can look to microorganisms for examples of beating, rotating, and waving motions that break time symmetry to allow forward propulsion. In particular, the undulating waves created on the surface of ciliates are time-irreversible and provide a net propulsive force. This mechanism has been simply modeled as a

swimming sheet.<sup>17</sup> In this Letter, we construct and analyze millimeter-scale swimming sheet robots with a continuous magnetization profile, driven by applied magnetic fields.

Swimming micro-robots have been developed by using magnetically driven rotating helical tails,<sup>14</sup> beating flagellar motion,<sup>11</sup> and, at the centimeter-scale, discretized traveling waves.<sup>13</sup> However, true traveling waves at or under the millimeter scale have not been shown experimentally due to actuation limitations. Traveling wave undulatory swimming, analogous to the motion of beating cilia, only requires wave deformation in two dimensions (2D) and thus is well suited for a demonstration using soft micro-robotics with programmable magnetic actuation. The fluid dynamics of such swimming patterns have been studied extensively.<sup>17–21</sup>

This Letter presents a robot that can generate a true traveling-wave deformation along the length of its body using a spatially varying magnetization profile when actuated by an external rotating magnetic field. The magnetization profile is given by the vector  $\mathbf{M}(x)$  which varies continuously along the length of the device, parameterized by the variable  $x$ . Prototype devices are constructed from the permanent magnet material neodymium-iron-boron (NdFeB, density  $\rho = 7.6 \text{ g/cm}^3$ , Magnequench), which has a high saturation magnetization, and platinum-cure silicon rubber (Ecoflex 0050, density  $\rho = 1.07 \text{ g/cm}^3$ , Young's modulus  $E = 83 \text{ kPa}$ ). NdFeB particles, ground to a size of approximately  $10\text{--}50 \mu\text{m}$  in diameter using a ball mill, were mixed with the Ecoflex at a mass ratio of 1:1. A sheet is formed by pressing the mixture of Ecoflex and magnetic particles between two glass slides during the curing process, yielding a thickness around  $50 \mu\text{m}$  determined by spacers. The sheet is easily cut into millimeter-scale strips and the presented prototype has dimensions of 1.9 mm by 5.9 mm. The magnetization procedure is shown in Figs. 1(a)–1(d). The flexible elastomeric magnetic strip is bent into a circle and placed in a uniform 1 T magnetic field oriented perpendicular to the circle's axis. Once removed from the field and straightened, this leads to a magnetization profile within the sheet given by

<sup>a)</sup>E. Diller and J. Zhuang contributed equally to this work.

<sup>b)</sup>Author to whom correspondence should be addressed. Electronic mail: [sitti@cmu.edu](mailto:sitti@cmu.edu)

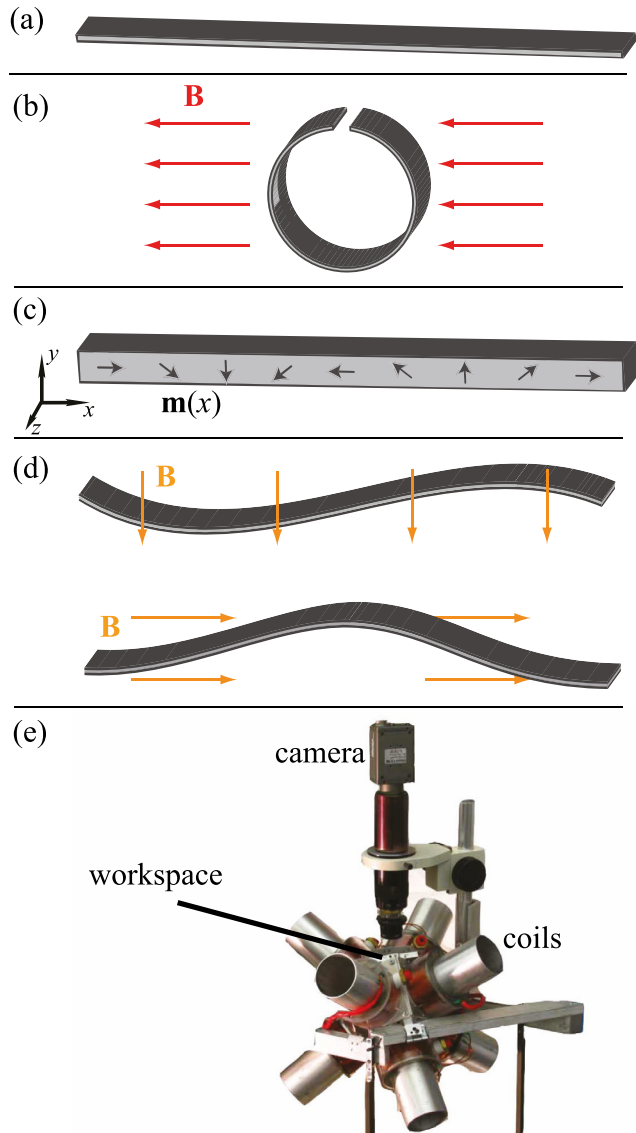


FIG. 1. The fabrication, magnetization, and actuation process of a swimming-sheet milli-robot. (a) A flat sheet fabricated from permanent magnetic particles and Ecoflex is (b) bent into a circle and subject to a 1 T uniform magnetic field. (c) When the field is removed and the robot straightened, it is left with a magnetization that varies along its length, which (d) causes it to be deformed when subject to a weak external field. Rotating the external field continuously in time causes the sheet deformations to travel down its length, providing a propulsive force in fluid. (e) The magnetic coil system for generating the rotating field.

$$\mathbf{M}(x) = M \cos\left(\frac{2\pi x}{\lambda}\right) \mathbf{i} - M \sin\left(\frac{2\pi x}{\lambda}\right) \mathbf{j}. \quad (1)$$

Here,  $M$  is the magnetization magnitude,  $\lambda$  represents the wavelength of the sinusoidal deformation, and  $\mathbf{i}$  and  $\mathbf{j}$  are the unit vectors along the  $x$  and  $y$  axes, respectively. Different magnetization profiles can be achieved by varying the shape and size of the strip during the magnetization step. For example, the wavelength of the device in Fig. 1(d) is equal to the circumference of the circle in Fig. 1(b). After the device is straightened, it can be deformed (Fig. 1(d)) by a low-strength uniform magnetic field generated by a magnetic coil system (Fig. 1(e)). The magnetization profile  $\mathbf{M}(x)$  will not be

remagnetized by the actuating field, 1–10 mT, as it is much lower than the coercivity of the NdFeB ( $\sim 780$  mT). The device we present has a wavelength of 4.0 mm and a measured magnetization magnitude of  $M = 2.35 \times 10^{-3}$  emu/cm<sup>3</sup> (measured in an alternating gradient force magnetometer).

When a magnetic field in the  $x$ - $y$  plane,  $\mathbf{B}$ , is applied, the milli-robot will experience a magnetic moment along its width in the  $z$  direction,  $\tau(x)$ . This moment will vary along the length of the milli-robot depending on  $\mathbf{B}$  and the local direction of  $\mathbf{M}(x)$ . Assuming small deflections, the applied torque at position  $x$ ,  $\tau(x)$ , is given by

$$\tau(x) = \int_0^x \mathbf{M}(x) \times \mathbf{B} A dx. \quad (2)$$

Here,  $A$  is the cross-sectional area of the milli-robot and  $\mathbf{k}$  is the unit vector in the  $z$ -direction. Assuming small deflection, the milli-robot deformation is found by solving the Euler-Bernoulli equation to be sinusoidal with amplitude  $b$  as

$$b = \frac{MA\lambda^3}{8\pi^3 EI} B, \quad (3)$$

where  $I$  is the beam's second moment of inertia.

A magnetic field rotating in the  $x$ - $y$  plane will result in a traveling sinusoidal deformation along the milli-robot length. The speed of the traveling wave,  $v_w$ , is the product of  $\lambda$  and the rotation frequency  $f$ . Assuming  $b \ll \lambda$  and that the sheet is inextensible, Taylor's model<sup>17</sup> gives the approximate swimming speed of the robot as

$$v = \frac{2\pi^2 b^2}{\lambda} f. \quad (4)$$

Taylor's model provides an approximate solution of the Stokes equation for an inextensible undulating boundary and is only truly applicable for  $Re \ll 1$ . In our case, the assumptions only weakly holds: the robot has a finite stiffness and is slightly extensible, at some conditions the deformations are not negligibly small, and the Reynolds number is of order 1. Furthermore, boundary effects from nearby container walls may play a role in the tested swimming conditions. However, we believe this simple model captures the fundamental dynamics of the system and gives a first order approximation of the relationship between field strength, field frequency, and the speed of the milli-robot. It is also relevant to the proposed scaling down of the presented swimmer.

A traveling transverse wave can be observed in Fig. 2(a), where the milli-robot is actuated by a 2 mT rotating field with a frequency of 1 Hz. With a continuously propagating wave, the robot can propel itself at a constant speed on the water surface or underwater near the bottom surface. When the milli-robot is restricted by surface tension to the water surface, two-dimensional (2D) control is readily achievable by changing the rotational axis of the driving field. As shown in Fig. 2(b), we can drive the robot along the predefined path "CMU" (see the supplementary video for the undulatory deformation and path tracking of the robot). Directional control can also be achieved for underwater motion, but the additional rotational degree of freedom makes control more difficult and operator-directed open-loop

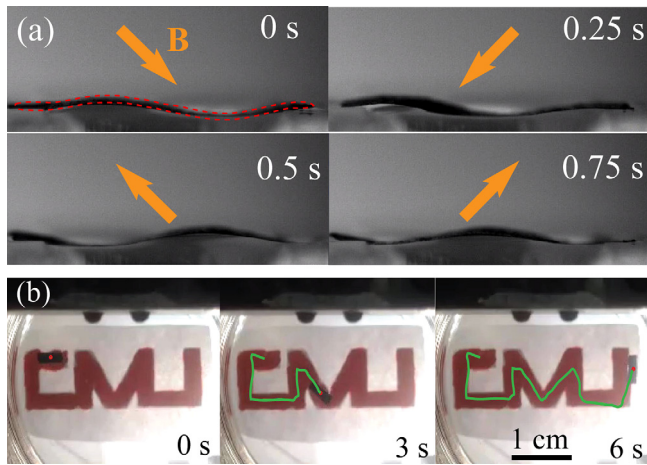


FIG. 2. (a) Propagating wave along the robot, where the dark stripe (marked by the dashed contour in the first frame) is the side view of the deformed robot. As the magnetic field  $\mathbf{B}$  rotates clockwise, the transverse harmonic deformation wave propagates from the left to the right hand side. (b) Controlled path following of the robot on the water surface. (Multimedia view) [URL: <http://dx.doi.org/10.1063/1.4874306.1>]

control has not been feasible. We believe that a closed-loop control system could reduce error to an acceptable level. Robust steering can also be achieved by adding a small magnetization bias to the robot which allows for steering with a corresponding field bias direction.

To characterize the deformation and swimming mechanism of the robot, we measure the deformation amplitude in quasi-static state at different applied field magnitudes. The robot is actuated by a slow rotating field (1 Hz) and its translational motion is restricted by an enclosure slightly larger than the dimensions of the milli-robot. As shown in Fig. 3, we find a linear relationship between deformation amplitude and actuating field strength. The slope of the line is a critical coefficient representing the magnetic-induced deformation stiffness of the robot. The measured results show agreement with the derived deformation model (Eq. (3)). At stronger actuating fields ( $>3$  mT), we expect a non-linear relationship to emerge as the small deformation approximation of Eq. (3) is violated.

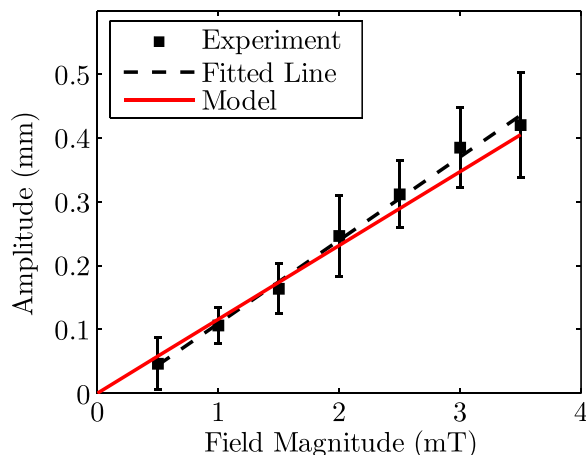


FIG. 3. Deformation of the milli-robot versus field magnitude at a rotational frequency of 1 Hz. The deformation amplitude is half of the peak-to-peak distance, measured directly from deformation images. The plotted model is based on Eq. (3).

We present results for this prototype swimming on the water surface and underwater near the bottom surface. For both conditions, we present the milli-robot's swimming speed with respect to the frequency and magnitude of the rotating magnetic field and compare our results with Taylor's model, as shown in Fig. 4.

Figs. 4(a) and 4(b) show the swimming speed versus frequency and magnitude on the water surface; Figs. 4(c) and 4(d) are analogous results for underwater near-bottom swimming. The speeds in Figs. 4(a) and 4(c) are measured at fixed field magnitudes of 2.5 mT and 2.0 mT, respectively. Speeds in Figs. 4(b) and 4(d) are measured at a constant rotational frequency of 30 Hz.

In the water surface case, we see an approximately linear relationship between swimming speed and frequency in both the experimental data and the model results; the disagreement between the slopes is mostly due to the fact that the sheet is only in contact with water on one side while Taylor's model requires the sheet immersed in the fluid. In the underwater case, there is no strong linear dependence of the speed on the actuating frequency. The discrepancy is attributed to wall effects, which are not taken into account in the fluid propulsion model used here. A full theoretical characterization of the near-wall fluid and contact friction effects is outside the scope of this study. At smaller field amplitudes, Taylor's model predicts the speed of the device along the surface as magnetic field strength changes, but as the field magnitude grows, large deformation and saturation of the deformation violate the linear model. Acceptable agreement between experiment and Taylor's model is seen in Fig. 4(d); at stronger actuating fields, a saturation of speed can be observed due to non-linear deformation behavior.

In summary, we have fabricated a millimeter-scale robot which emulates the undulatory traveling-wave swimming

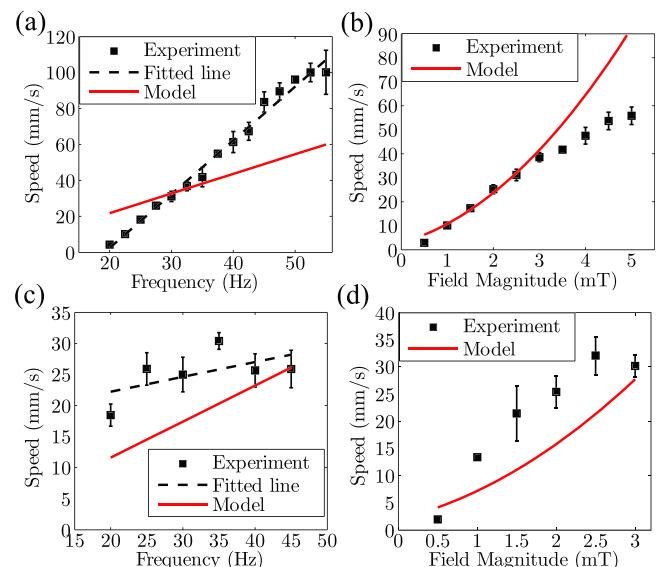


FIG. 4. Variation of robot swimming speed with field frequency and strength. Dependence of swimming speed on (a) field frequency and (b) field amplitude on water surface. Dependence of swimming speed on (c) field frequency and (d) field amplitude in the underwater case. In (a) and (c), the robot is actuated by constant field magnitudes of 2.5 mT and 2.0 mT, respectively. The frequency of magnetic field is kept constant in (b) and (d) at 30 Hz. The plotted model is based on Eq. (4).

observed in certain types of ciliated organisms. Traveling wave deformation is induced in the robot using a continuous magnetization profile and a flexible body. The elastomeric composite robot is magnetized so that in a rotating magnetic field it deforms in a traveling sinusoidal wave, providing a net propulsive force at low Reynolds number. The presented swimmer demonstrates the first distributed magnetization profile used to induce continuous deformation and actuation in a low Reynolds number swimmer. We measure the dependence of robot speed on field frequency and strength in both the surface and underwater swimming cases. We also use Taylor's swimming sheet model to provide first-order relationships between the field strength, field frequency, and swimming speeds. The swimming speed we demonstrate in this unoptimized prototype (up to 17 body-lengths per second for our swimmer of length 5.9 mm) is similar to that exhibited in other artificial<sup>12</sup> (magnetic flagella, 20 body-lengths per second) and biological<sup>22</sup> (*E. coli* bacteria, 10 body-lengths per second) micro-swimmers, suggesting that the method presented may prove viable for wider applications. The actuation principle should allow this type of milli-robot to be reduced in size to the micrometer length scale. Patterned magnetization with micrometer-scale resolution is used in magnetic data recording,<sup>23</sup> and such patterning techniques could be adapted to miniaturize the swimmers demonstrated in this work. With the use of colloidal magnetic nano-particles,<sup>11</sup> there are not expected to be any fundamental limitations on scaling to the single-micron size if appropriate fabrication methods can be achieved. When the swimmer is scaled down in size, its *Re* decreases and thus the analytical swimming model presented in this work will become even more accurate. Small-scale soft, controllable robots of this type could have potential applications in medicine, bioengineering, or microfluidic tasks.

M. R. Edwards was supported by an NSF Graduate Research Fellowship (Grant No. 09468251).

- <sup>1</sup>M. Sitti, *Nature* **458**, 1121–1122 (2009).
- <sup>2</sup>J. Edd, S. Payen, B. Rubinsky, M. Stoller, and M. Sitti, in *International Conference on Intelligent Robots and Systems*, 2003, pp. 2583–2588.
- <sup>3</sup>D. B. Weibel, P. Garstecki, D. Ryan, W. R. DiLuzio, M. Mayer, J. E. Seto, and G. M. Whitesides, *Proc. Natl. Acad. Sci. U. S. A.* **102**, 11963–11967 (2005).
- <sup>4</sup>B. Behkam and M. Sitti, *ASME J. Dyn. Syst. Meas. Control* **128**, 36–43 (2006).
- <sup>5</sup>M. R. Edwards, R. W. Carlsen, and M. Sitti, *Appl. Phys. Lett.* **102**, 143701 (2013).
- <sup>6</sup>B. J. Williams, S. V. Anand, J. Rajagopalan, and M. T. A. Saif, *Nature Commun.* **5**, 1–8 (2014).
- <sup>7</sup>D. Kim, A. Liu, E. Diller, and M. Sitti, *Biomed. Microdevices* **14**, 1009–1017 (2012).
- <sup>8</sup>S. Martel, M. Mohammadi, O. Felfoul, Z. Lu, and P. Pouponneau, *Int. J. Rob. Res.* **28**(4), 571–582 (2009).
- <sup>9</sup>A. Solovev, W. Xi, D. H. Gracias, S. M. Harazim, C. Deneke, S. Sanchez, and O. G. Schmidt, *ACS Nano* **6**, 1751–1756 (2012).
- <sup>10</sup>M. Xiao, X. Guo, M. Cheng, G. Ju, Y. Zhang, and F. Shi, *Small* **10**(5), 859–865 (2014).
- <sup>11</sup>R. Dreyfus, J. Baudry, M. L. Roper, M. Fermigier, H. A. Stone, and J. Bibette, *Nature* **437**, 862–865 (2005).
- <sup>12</sup>L. Zhang, K. E. Peyer, and B. J. Nelson, *Lab Chip* **10**, 2203–2215 (2010).
- <sup>13</sup>N. T. Jafferis, H. Stone, and J. C. Sturm, *Appl. Phys. Lett.* **99**, 114102 (2011).
- <sup>14</sup>S. Tottori, L. Zhang, F. Qiu, K. K. Krawczyk, A. Franco-Obregón, and B. J. Nelson, *Adv. Mater.* **24**, 811–816 (2012).
- <sup>15</sup>Z. Ye, S. Regnier, and M. Sitti, *IEEE Trans. Rob.* **30**, 3–13 (2014).
- <sup>16</sup>J. J. Abbott, K. E. Peyer, M. C. Lagomarsino, L. Zhang, L. Dong, I. K. Kaliakatos, and B. J. Nelson, *Int. J. Rob. Res.* **28**, 1434 (2009).
- <sup>17</sup>G. Taylor, *Proc. R. Soc. A* **209**, 447–461 (1951).
- <sup>18</sup>E. O. Tuck, *J. Fluid Mech.* **31**, 305–308 (1968).
- <sup>19</sup>O. S. Pak and E. Lauga, *Proc. R. Soc. A* **466**, 107–126 (2010).
- <sup>20</sup>E. Lauga and T. R. Powers, *Rep. Prog. Phys.* **72**, 096601 (2009).
- <sup>21</sup>M. Sauzade, G. J. Elfring, and E. Lauga, *Physica D: Nonlinear Phenomena* **240**, 1567–1573 (2011).
- <sup>22</sup>N. C. Darnton, L. Turner, S. Rojevsky, and H. C. Berg, *J. Bacteriol.* **189**(5), 1756–1764 (2007).
- <sup>23</sup>N. Thompson and J. Best, *IBM J. Res. Dev.* **44**(3), 311–322 (2000).